Mineralogical Magazine (2023), **87**, 151–159
doi:10.1180/mgm.2022.106

CAMBRIDGE UNIVERSITY PRESS

Article

Oldsite, $K_2Fe^{2+}[(UO_2)(SO_4)_2]_2(H_2O)_8$, a new uranyl sulfate mineral from Utah, USA: its description and implications for the formation and occurrences of uranyl sulfate minerals

Jakub Plášil[1]*, Anthony R. Kampf[2], Chi Ma[3] and Joy Desor[4]

[1]Institute of Physics ASCR, v.v.i., Na Slovance 1999/2, 18221 Prague 8, Czech Republic; [2]Mineral Sciences Department, Natural History Museum of Los Angeles County, 900 Exposition Boulevard, Los Angeles, CA 90007, USA; [3]Division of Geological and Planetary Sciences, California Institute of Technology, Pasadena, California 91125, USA; and [4]Independent Researcher, Bad Homburg, Germany

Abstract

Oldsite (IMA2021-075), ideally $K_2Fe^{2+}[(UO_2)(SO_4)_2]_2(H_2O)_8$, is a new uranyl sulfate mineral found on specimens from the North Mesa Mine group, Temple Mountain, San Rafael district, Emery County, Utah, USA. It is a secondary mineral occurring with alum-(K), halotrichite, metavoltine, quartz, römerite, stanleyite, sulphur, szomolnokite and mathesiusite. It forms rectangular blades flattened on {010} and elongated on [001], reaching ~0.3 mm in length. Crystals are yellow in colour, transparent with a vitreous lustre; the streak is very pale yellow. The mineral is non-fluorescent. Cleavage is excellent on {100} and perfect on {010}; the Mohs hardness is ~2. Crystals are brittle with irregular, splintery fracture. The density measured by flotation in a mixture of methylene iodide and toluene is 3.31 g·cm^{-3}; the calculated density is 3.298 g·cm^{-3} for the empirical formula and 3.330 g·cm^{-3} for the ideal formula. Oldsite is biaxial (+), with $\alpha = 1.552(2)$, $\beta = 1.556(2)$ and $\gamma = 1.588(2)$ (measured in white light). The 2V measured directly on a spindle stage is 37(1)°; the calculated 2V is 39.6°. Dispersion is $r < v$, moderate. The optical orientation is $X = \mathbf{b}$, $Y = \mathbf{a}$ and $Z = \mathbf{c}$. The mineral is non-pleochroic. The empirical formula of oldsite (on the basis of 28 O apfu) is $K_{1.93}(Fe^{2+}_{0.53}Zn_{0.31}V^{3+}_{0.09}Mg_{0.08})_{\Sigma 1.02}[(U_{0.98}O_2)(S_{1.01}O_4)_2]_2(H_2O)_8$. The Raman spectrum is dominated by the vibrations of SO_4^{2-} and UO_2^{2+} units. Oldsite is orthorhombic, $Pmn2_1$, $a = 12.893(3)$, $b = 8.276(2)$, $c = 11.239(2)$ Å, $V = 1199.2(5)$ Å^3 and $Z = 2$. The five strongest powder X-ray diffraction lines are [d_{obs}, Å (*I*, %) (*hkl*)]: 8.29 (59) (010), 6.47 (82) (200), 5.10 (62) (210), 4.65 (100) (012, 211) and 3.332 (55) (022, 221). The crystal structure of oldsite was refined from single-crystal X-ray data to $R = 0.0258$ for 2676 independent observed reflections, with $I_{obs} > 3\sigma(I)$. Oldsite is an Fe^{2+} analogue of svornostite; its crystal structure is based upon infinite chains of uranyl-sulfate polyhedra, which comprises pentagonal UO_7 bipyramids sharing four of their equatorial vertices with sulfate tetrahedra such that each tetrahedron is linked to two uranyl bipyramids to form an infinite chain (the free, non-linking equatorial vertex of the uranyl bipyramid is an H_2O group). The broader discussion on the origin and composition of uranyl sulfate minerals is made. The new mineral name honours American mineralogist, Dr. Travis A. Olds for his contribution to uranium mineralogy.

Keywords: oldsite, new mineral, uranyl sulfate, crystal structure, Raman spectroscopy, North Mesa mines, Emery County, Utah, USA, supergene weathering

(Received 9 June 2022; accepted 31 August 2022; Accepted Manuscript published online: 8 September 2022; Associate Editor: Michael Rumsey)

Introduction

Over the last ten years, the quest for new uranyl minerals in inactive uranium mines, especially in Jáchymov, Czech Republic and the Red Canyon, southeastern Utah, USA, has proven remarkably successful. There are optimal conditions for the growth of secondary minerals in the abandoned mining adits and tunnels due to high relative air humidity and stable temperatures. The complex specific geochemistry at both localities (see the Discussion section) has led to the formation of more than 30 new uranyl sulfates that have been collected from efflorescent encrustations on tunnel walls and characterised as valid minerals (see, e.g. Škácha *et al.*, 2019; Kampf *et al.*, 2021 and references therein). Crystallographic studies on these minerals have revealed some exciting features not previously observed in natural or synthetic phases (Gurzhiy and Plášil, 2019). New types of clusters, chains and sheets of polyhedra were identified. The great diversity observed for uranyl sulfate minerals stems primarily from many possible linkages between uranyl coordination polyhedra and sulfate tetrahedra. Here, we describe a new uranyl sulfate, oldsite, an Fe^{2+}-analogue of svornostite (Plášil *et al.*, 2015b). It has been

*Author for correspondence: Jakub Plášil, Email: plasil@fzu.cz
Cite this article: Plášil J., Kampf A.R., Ma C. and Desor J. (2023) Oldsite, $K_2Fe^{2+}[(UO_2)(SO_4)_2]_2(H_2O)_8$, a new uranyl sulfate mineral from Utah, USA: its description and implications for the formation and occurrences of uranyl sulfate minerals. *Mineralogical Magazine* **87**, 151–159. https://doi.org/10.1180/mgm.2022.106

found at the North Mesa Mine group, Temple Mountain, San Rafael district, Emery County, Utah, USA and was approved by the Commission on New Minerals, Nomenclature and Classification of the International Mineralogical Association (IMA2021-075, Plášil *et al.*, 2021). The description is based on one holotype specimen deposited in the collections of the Natural History Museum of Los Angeles County, 900 Exposition Boulevard, Los Angeles, CA 90007, USA, catalogue number 76159. The new mineral is named after American mineralogist Travis A. Olds (born 1990), currently curator at the Carnegie Museum of Natural History in Pittsburgh, in recognition of his contributions to uranium mineralogy and crystallography. Dr. Olds' research is focused on the descriptive mineralogy and crystal chemistry of secondary minerals and hexavalent uranium. He has been involved in the description of more than 24 new minerals, of which 21 contain uranium.

Occurrence

Oldsite was discovered on specimens collected from the North Mesa mine group by one of the authors (JD). In the mines of the North Mesa mine group, ore occurs in lenses of conglomeratic sandstone, scattered nodules in the sandstone, and in massive layers in the conglomerate near its contacts with other rocks. Near the base of the Shinarump conglomerate, high-grade asphaltic ore, with galena and sphalerite, occurs in silicified and calcified logs (Schindler *et al.*, 2003). Oldsite is a post-mining alteration product resulting from the oxidation of primary ores in the humid underground environment and subsequent deposition with a variety of secondary minerals forming efflorescent crusts on the surfaces of mine walls. Oldsite has been found on pyrite-rich asphaltite at the contact zone of the U–V mineralised sandstone. The mineral association comprises alum-(K), halotrichite, metavoltine, quartz, römerite, stanleyite, sulphur, szomolnokite and mathesiusite.

Physical and optical properties

Oldsite crystals are rectangular blades flattened on {010} and elongated on [001]. The crystal forms observed were {100}, {010}, {001}, {00$\bar{1}$} and possibly {101} and/or {102}. Crystals, up to ~0.3 mm in length, occur as isolated individuals and in subparallel to divergent groups (Fig. 1). The mineral is yellow in colour and transparent with a vitreous lustre. Its streak is very pale yellow. The mineral is non-fluorescent. The Mohs hardness is ~2, by analogy with svornostite. Crystals are brittle with irregular, splintery fracture. Cleavage is excellent on {100} and perfect on {010}. Oldsite dissolves readily in room-temperature H_2O. The density measured by flotation in a mixture of methylene iodide and toluene is 3.31 g·cm^{-3}; the calculated density is 3.298 g·cm^{-3} for the empirical formula and 3.330 g·cm^{-3} for the ideal formula.

Fig. 1. Diverging group of yellow oldsite blades with blue stanleyite and white szomolnokite on asphaltum. The field of view is 0.68 mm across.

Optically, oldsite is biaxial (+), with $\alpha = 1.552(2)$, $\beta = 1.556(2)$ and $\gamma = 1.588(2)$ (measured in white light). The 2V measured directly on a spindle stage is 37(1)°; the calculated 2V is 39.6°. Dispersion is $r < v$, moderate. The optical orientation is $X = \mathbf{b}$, $Y = \mathbf{a}$ and $Z = \mathbf{c}$. The mineral is non-pleochroic. The Gladstone–Dale compatibility index $1 - (K_P/K_C)$ for the empirical formula is −0.001, in the superior range (Mandarino, 2007), using $k(UO_3) = 0.118$, as provided by Mandarino (1976) and 0.005 (also superior) for the ideal formula.

Raman spectroscopy

Raman spectroscopy was conducted on a Horiba XploRA PLUS using a 532 nm diode laser, a 100 μm slit, a 1800 gr/mm diffraction grating and a 100× (0.9 NA) objective. The Raman spectrum of oldsite from 4000 to 60 cm^{-1} is shown in Fig. 2.

Raman bands at 3620, 3546 and 3498 cm^{-1} are attributed to υ O–H stretching vibrations of symmetrically non-equivalent H_2O molecules. The inferred O–H···O hydrogen bond lengths, using the empirical relation given by Libowitzky (1999), vary in the range ~3.2 to 2.9 Å. A very weak band at 1618 cm^{-1} (too weak to see in Fig. 2) is attributable to υ_2 (δ) H–O–H bending vibrations. Bands at 1218, 1192 and 1154 cm^{-1} are attributed to triply degenerate υ_3 (SO_4^{2-}) antisymmetric stretching vibrations and those at 1040, 1025, 1002 and 986 cm^{-1} to υ_1 (SO_4^{2-}) symmetric stretching vibrations. (Those have higher relative intensity compared to υ_3, which is in line with the general behaviour of symmetrical modes in Raman.) A very weak band at 952 cm^{-1} and a very strong one at 859 cm^{-1} are assigned to υ_3 $(UO_2)^{2+}$ antisymmetric and υ_1 (UO_2^{2+}) symmetric stretching vibrations. The approximate U–O bond length inferred from the respective wavenumbers of the UO_2^{2+} vibrations after Bartlett and Cooney (1989) is ~1.76 Å, which is in line with the structure determination (see below). Bands at 642 and 592 cm^{-1} are attributed to triply degenerate υ_4 (δ) (SO_4^{2-}) bending vibrations. A doublet at 463 and 446 cm^{-1} is assigned to υ_2 (δ) (SO_4^{2-}) bending vibrations. A weak band at 329 cm^{-1} can be assigned to the υ ($U–O_{ligand}$) vibrations. A band of medium intensity at 186 cm^{-1} with shoulders can be assigned to split, doubly degenerate υ_2 (δ) (UO_2^{2+}) bending vibrations. Bands at 88 (shoulder) and 75 cm^{-1} are attributable to lattice vibrations.

Chemical composition

Analyses of oldsite (4 points) were performed at Caltech on a JEOL 8200 electron microprobe in wavelength dispersive spectroscopy mode. Oldsite crystals are too thin and fragile to polish, so the blades were mounted on carbon tape and carbon coated; the analyses were then done on unpolished crystal faces. The mineral is very beam-sensitive. Analytical conditions were 15 kV accelerating voltage, 2 nA beam current and a 15 μm beam diameter. Insufficient pure material is available for CHN or thermal gravimetric analysis; however, the fully ordered structure

https://doi.org/10.1180/mgm.2022.106 Published online by Cambridge University Press

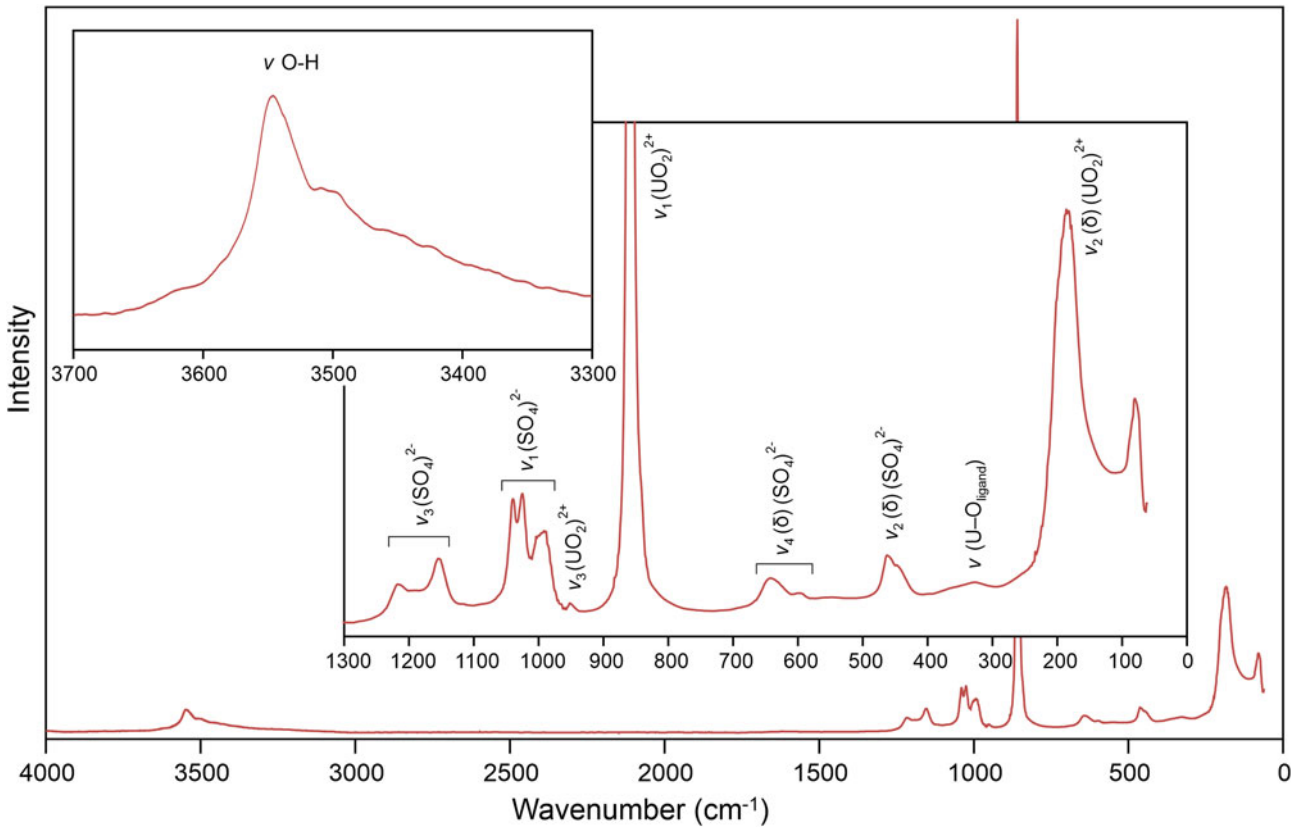

Fig. 2. Raman spectrum of oldsite recorded with a 532 nm laser.

unambiguously established the quantitative content of H_2O. The beam sensitivity of the mineral and analyses conducted on flat but slightly uneven crystal faces accounts for the low analytical total. Analytical data are given in Table 1. The empirical formula (calculated on the basis of 28 O atoms per formula unit) is $K_{1.93}(Fe^{2+}_{0.53}Zn_{0.31}V^{3+}_{0.09}Mg_{0.08})_{\Sigma 1.02}[(U_{0.98}O_2)(S_{1.01}O_4)_2]_2(H_2O)_8$. The ideal formula is $K_2Fe^{2+}(UO_2)_2(SO_4)_4(H_2O)_8$, which requires K_2O 7.83, FeO 5.97, UO_3 47.57, SO_3 26.63, H_2O 11.99, total 100 wt. %.

X-ray crystallography and structure refinement

Powder X-ray diffraction was done using a Rigaku R-Axis Rapid II curved imaging plate microdiffractometer, with monochromatised Mo*K*α radiation. A Gandolfi-like motion on the φ and ω axes was used to randomise the sample and observed *d*-values and intensities were derived by profile fitting using *JADE Pro* software (Materials Data, Inc.). The powder data are presented in Supplementary Table S1 (available as Supplementary material, see below).

The single-crystal structure data were collected at room temperature using a Rigaku SuperNova diffractometer equipped with Atlas S2 CCD detector and a microfocus source utilising monochromated Mo*K*α radiation. The crystallographic properties and the experimental and refinement details are given in Table 2. The *CrysAlis* software was used for data processing, including application of an empirical multi-scan absorption correction. The structure was solved using the intrinsic phasing algorithm of the *SHELXT* program (Sheldrick, 2015). Refinement proceeded by full-matrix least-squares on F^2 using *Jana2020* (Petříček *et al.*, 2020). The structure solution found all non-hydrogen atom sites; U, S and Fe atoms were refined to full occupancy with anisotropic displacement parameters; O atoms were refined with isotropic displacement parameters; H atoms could not be found using the current data. As the structure crystallises in a non-centrosymmetric orthorhombic space group, an inversion twin was implemented in the refinement, giving a slightly negative Flack parameter and, thereby, confirming the dominance of one enantiomer present in the studied crystal. Atom coordinates and displacement parameters are given in Table 3, selected bond-distances in Table 4 and a bond-valence analysis in Table 5. The crystallographic information file has been deposited with the Principal Editor of *Mineralogical Magazine* and is available as Supplementary material (see below).

Table 1. Chemical composition (wt.%) for oldsite.

Constituent	Mean	Range	S.D.	Standard
K_2O	7.47	7.38–7.58	0.09	microcline
FeO	3.16	2.94–3.40	0.19	fayalite
ZnO	2.10	1.74–2.38	0.32	ZnO
MgO	0.27	0.19–0.33	0.06	forsterite
V_2O_3	0.53	0.50–0.58	0.04	V_2O_5
UO_3	45.90	45.18–46.43	0.59	UO_2
SO_3	26.46	26.33–26.65	0.14	anhydrite
H_2O*	11.87			
Total	97.76			

* Based on the structure.
S.D. – standard deviation

Description and discussion of the structure

The structure of oldsite contains one U, two S, one Fe, two K and 18 O sites in the asymmetric unit. The U site is surrounded by seven O atoms forming an UO_7 pentagonal bipyramid, the typical

https://doi.org/10.1180/mgm.2022.106 Published online by Cambridge University Press

Table 2. Data collection and structure refinement details for oldsite.

Crystal data	
Structural formula	$K_{1.86}Fe[(UO_2)(SO_4)_2]_2(H_2O)_8$
Unit-cell parameters:	
a, *b*, *c* (Å)	12.893(3), 8.276(2), 11.239(2)
V (Å^3)	1199.2(5)
Z	2
Space group	$Pmn2_1$
D_{calc} (g cm^{-3})	3.269 (without H atoms)
Temperature	298 K
Data collection	
Wavelength	Mo*K*α, 0.71073 Å
Crystal dimensions (mm)	0.036 × 0.023 × 0.007
Collection mode	ω scans to fill an Ewald sphere
Frame width, counting time	1.0, 340 s
Limiting θ angles (°)	2.40–29.49°
Limiting Miller indices	$-17 \le h \le 17$, $-11 \le k \le 11$, $-14 \le l \le 15$
No. of reflections	30,517
No. of unique reflections	3271
No. of observed reflections (criterion)	2676 [$I > 3\sigma(I)$]
Absorption correction (mm^{-1}), method	14.86, multi-scan
T_{min}/T_{max}	0.626/1.00
R_{int}	0.043
F_{000}	1072
Refinement	
Refinement method	Jana2020 on F^2
Parameters, constraints, restraints	111, 1, 0
R_1, wR_2 (obs)	0.0258, 0.0628
R_1, wR_2 (all)	0.0383, 0.0691
GOF (obs, all)	1.05, 1.04
Weighting scheme, weights	σ, $1/(\sigma^2(F) + 0.00148F^2)$
$\Delta\rho_{min}$, $\Delta\rho_{max}$ (*e*.Å^{-3})	−1.12, 1.56
Flack parameter/Friedel pairs	−0.003(9)/1502

Table 4. Selected bond distances (Å) for oldsite.

U1–O4	2.494(4)	S1–O5	1.472(6)
U1–O7	2.362(5)	S1–O7	1.498(6)
U1–O8^{iii}	2.337(6)	S1–O13	1.445(5)
U1–O9	1.768(5)	S1–O16	1.503(6)
U1–O11	1.759(5)	<S1–O>	1.480
U1–O12^{ii}	2.381(6)		
U1–O16^{i}	2.379(5)	S2–O6	1.443(5)
<U1–O_{Ur}>	1.764	S2–O8	1.494(6)
<U1–O_{eq}>	2.391	S2–O12	1.481(6)
		S2–O14	1.442(6)
Fe1–O1	2.123(9)	<S2–O>	1.465
Fe1–O3	2.099(10)		
Fe1–O6	2.104(5)	K2–O2	2.832(11)
Fe1–O6^{iv}	2.104(5)	K2–O5	2.995(6)
Fe1–O15^{v}	2.117(11)	K2–O5^{xv}	2.995(6)
Fe1–O17	2.111(9)	K2–O10^{x}	2.860(9)
<Fe1–O>	2.110	K2–O11^{x}	3.286(6)
		K2–O11^{xvi}	3.286(6)
K1–O2^{viii}	3.667(10)	K2–O12^{vii}	2.976(5)
K1–O3^{vii}	3.355(9)	K2–O12^{xvii}	2.976(5)
K1–O9	2.907(6)	K2–O14^{vii}	3.158(6)
K1–O9^{ix}	2.907(6)	K2–O14^{xvii}	3.158(6)
K1–O10^{i}	3.107(10)	K2–O15	3.381(10)
K1–O13	2.810(6)	<K2–O>	3.082
K1–O13^{ix}	2.810(6)		
K1–O14^{iii}	2.755(6)		
K1–O14^{vi}	2.755(6)		
<K1–O>	3.008		

Symmetry codes = (i) −x + 3/2, −y + 1, z + 1/2; (ii) x + 1, y + 1, z + 1; (iii) −x + 1/2, −y, z + 3/2; (iv) −x, y, z; (v) −x + 1/2, −y, z − 3/2; (vi) x + 3/2, −y, z + 3/2; (vii) x + 1, y, z + 1; (viii) −x + 3/2, −y, z + 1/2; (ix) −x + 2, y, z; (x) x, y − 1, z; (xv) −x + 1, y, z; (xvi) −x + 1, y − 1, z; (xvii) −x, y, z + 1.

coordination for U^{6+} in which the two short apical bonds of the bipyramid constitute the uranyl group (see, e.g. Burns, 2005). Five equatorial O atoms (O_{eq}) complete the U coordination environment. The pentagonal UO_7 bipyramid shares four equatorial vertices with sulfate tetrahedra such that each tetrahedron is linked to two uranyl bipyramids to form an infinite chain. The free, non-linking equatorial vertex of the uranyl bipyramid is occupied by an H_2O molecule based on bond-valence calculations. The H-bonding *via* this H_2O molecule (O4 atom, Fig. 3a) weakly links the chains into a sheet-like structure. Such infinite chains

Table 3. Atom coordinates and displacement parameters (Å^2) for oldsite.[†]

	x/a	*y/b*	*z/c*	U_{iso}*/U_{eq}	U^{11}	U^{22}	U^{33}	U^{12}	U^{13}	U^{23}
U1	0.745297(14)	0.61324(2)	0.74956(4)	0.01172(6)	0.01410(11)	0.01181(11)	0.00924(11)	0.00088(8)	0.00112(14)	0.00012(18)
Fe1	0	−0.15971(17)	−0.55871(14)	0.0197(4)	0.0152(6)	0.0250(7)	0.0190(7)	0	0	0.0012(6)
K1	1	0.2727(3)	0.7304(2)	0.0330(9)	0.0187(12)	0.0492(17)	0.0312(19)	0	0	−0.0006(13)
K2	½	−0.1206(4)	0.5751(4)	0.0497(14)	0.0345(19)	0.044(2)	0.071(3)	0	0	0.0008(17)
S1	0.72756(14)	0.2581(3)	0.55816(19)	0.0140(5)	0.0182(7)	0.0137(9)	0.0100(9)	0.0011(8)	−0.0018(7)	0.0000(7)
S2	−0.25353(11)	−0.2436(3)	−0.5629(2)	0.0135(5)	0.0170(9)	0.0134(10)	0.0102(9)	−0.0013(6)	0.0000(6)	0.0004(7)
O1	0	0.0936(10)	−0.5870(9)	0.031(2)*						
O2	½	0.1133(12)	0.3913(11)	0.053(4)*						
O3	0	−0.1058(10)	−0.3762(9)	0.038(3)*						
O4	0.7936(4)	0.9042(5)	0.7332(5)	0.0254(11)*						
O5	0.6768(4)	0.1110(5)	0.6033(5)	0.0274(12)*						
O6	−0.1628(4)	−0.1415(6)	−0.5592(5)	0.0290(12)*						
O7	0.6869(4)	0.3967(5)	0.6301(5)	0.0241(12)*						
O8	−0.2225(5)	−0.4031(7)	−0.6140(6)	0.0406(16)*						
O9	0.8750(4)	0.5641(6)	0.7136(4)	0.0232(11)*						
O10	½	0.5598(11)	0.4778(9)	0.047(2)*						
O11	0.6162(4)	0.6657(6)	0.7824(4)	0.0236(11)*						
O12	−0.2912(4)	−0.2726(6)	−0.4403(5)	0.0232(10)*						
O13	0.8396(4)	0.2524(6)	0.5618(5)	0.0287(11)*						
O14	−0.3364(4)	−0.1714(6)	−0.6307(5)	0.0277(11)*						
O15	½	0.2058(9)	0.7563(10)	0.0457(19)*						
O16	0.6900(4)	0.2857(5)	0.4333(5)	0.0245(11)*						
O17	0	−0.4112(10)	−0.5265(8)	0.040(2)*						

[†]Refined occupancy for K1 and K2 are 0.932(9) and 0.928(11), respectively.

https://doi.org/10.1180/mgm.2022.106 Published online by Cambridge University Press

Table 5. Bond valence analysis for oldsite. Values are expressed in valence units*.

	U	Fe	K1	K2	S1	S2	Sum^{-H}	Assignment	Sum^{+H}	Theor[H]	nH$_2$O
O1		0.35					0.36	H_2O	1.96		1
O2			0.02	0.14			0.16	H_2O	1.76	1	1
O3		0.37	0.04				0.41	H_2O	2.01		1
O4	0.39						0.39	H_2O	1.99		2
O5				0.09×2↓	1.50		1.59	O		2	
O6		0.37×2↓				1.61	1.98	O			
O7	0.51				1.41		1.92	O			
O8	0.54					1.42	1.96	O			
O9	1.80		0.12×2↓				1.92	O			
O10			0.07	0.13			0.20	H_2O	1.80	1	1
O11	1.83			0.04×2↓			1.88	O		1	
O12	0.49			0.10		1.47	2.06	O			
O13			0.15×2↓		1.61		1.75	O		1	
O14			0.17×2↓	0.10×2↓		1.62	1.88	O		1	
O15		0.36		0.06			0.42	H_2O	2.02		1
O16	0.46				1.39		1.88	O		1	
O17		0.36					0.36	H_2O	1.96		1
Sum	6.06	2.20	0.99	0.89	5.91	6.12					8

* Bond valence parameters are from Gagné and Hawthorne (2015). sum^{-H} – the sum of the BV without the contribution of the H-bonds; sum^{+H} – the sum of the BV including assumed H-bonds (considering the theoretical H-bond strength of 0.8 vu; after Brown, 2002); theor[H] – theoretical number of additional weak H-bonds that the O atom could accept; nH$_2$O – number of H_2O molecules/cell considering site-multiplicities and $Z = 2$.

have been found in other uranyl sulfates, for instance, in svornostite (Plášil *et al.*, 2015b), bobcookite (Kampf *et al.*, 2015), rietveldite (Kampf *et al.*, 2017) and in the synthetic compounds $K_2[(UO_2)(SO_4)_2(H_2O)](H_2O)$ (Ling *et al.*, 2010) and $Mn(UO_2)(SO_4)_2(H_2O)_5$ (Tabachenko *et al.*, 1979). The Fe site is octahedrally coordinated by two O atoms and four H_2O groups. Each of the two O atoms of the Fe-octahedron is shared with SO_4 tetrahedra in a different chain, thereby linking adjacent chains. The long K–O bonds provide additional linkages between chains, involving either O atoms of the SO_4 groups or apical O atoms of the uranyl ion (Fig. 3b). The structural formula obtained from the refinement is $K_{1.86}Fe[(UO_2)(SO_4)_2]_2(H_2O)_8$. The lower refined occupation factors for both of K sites in the structure of oldsite lead to significant improvement of the fit (decrease of U_{eq} values and drop in *R*-factors). Nevertheless, the exact charge balancing mechanism (most probably *via* protonisation of some of the apical O atoms of the SO_4 tetrahedra) remains unclear based on the current data.

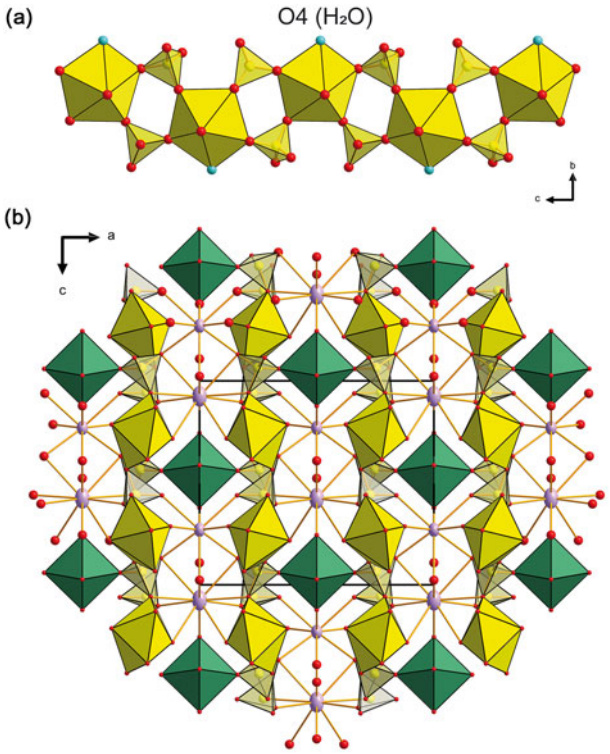

Fig. 3. Crystal structure of oldsite. (a) Part of the infinite uranyl sulfate chain found in the crystal structure of oldsite. UO_7 bipyramids are yellow, SO_4 tetrahedra light yellow (transparent), O atoms are red, except for the O4 atom (H_2O molecule) in aqua blue. (b) Structure viewed down [010]. Colour scheme as in (a); plus, Fe-octahedra green, K atoms lavender (and shown as thermal ellipsoids at 75% probability).

Discussion – chemical composition of uranyl sulfates, their formation and occurrence

Uranyl sulfate minerals form under oxidising conditions from aqueous solutions with high SO_4 activity. These conditions are typically related to the post-mining processes involving oxidative dissolution of sulfides, known as acid-mine-drainage (AMD) phenomena (e.g. Evangelou and Zhang, 1995; Edwards *et al.*, 2000; Brugger *et al.*, 2003; Plášil *et al.*, 2014). Although we now know

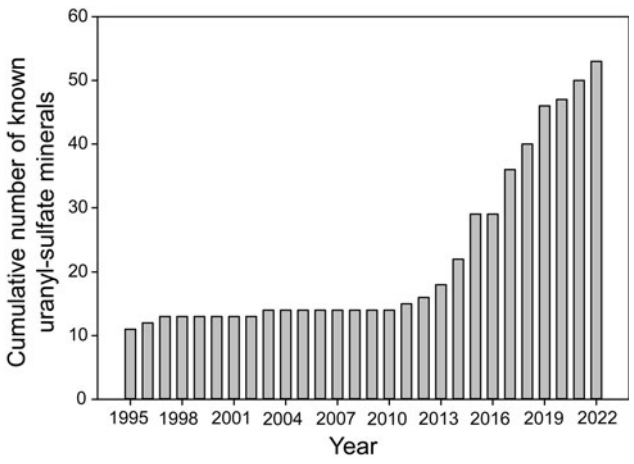

Fig. 4. Graph showing the rising number of known uranyl sulfate minerals throughout recent years.

https://doi.org/10.1180/mgm.2022.106 Published online by Cambridge University Press

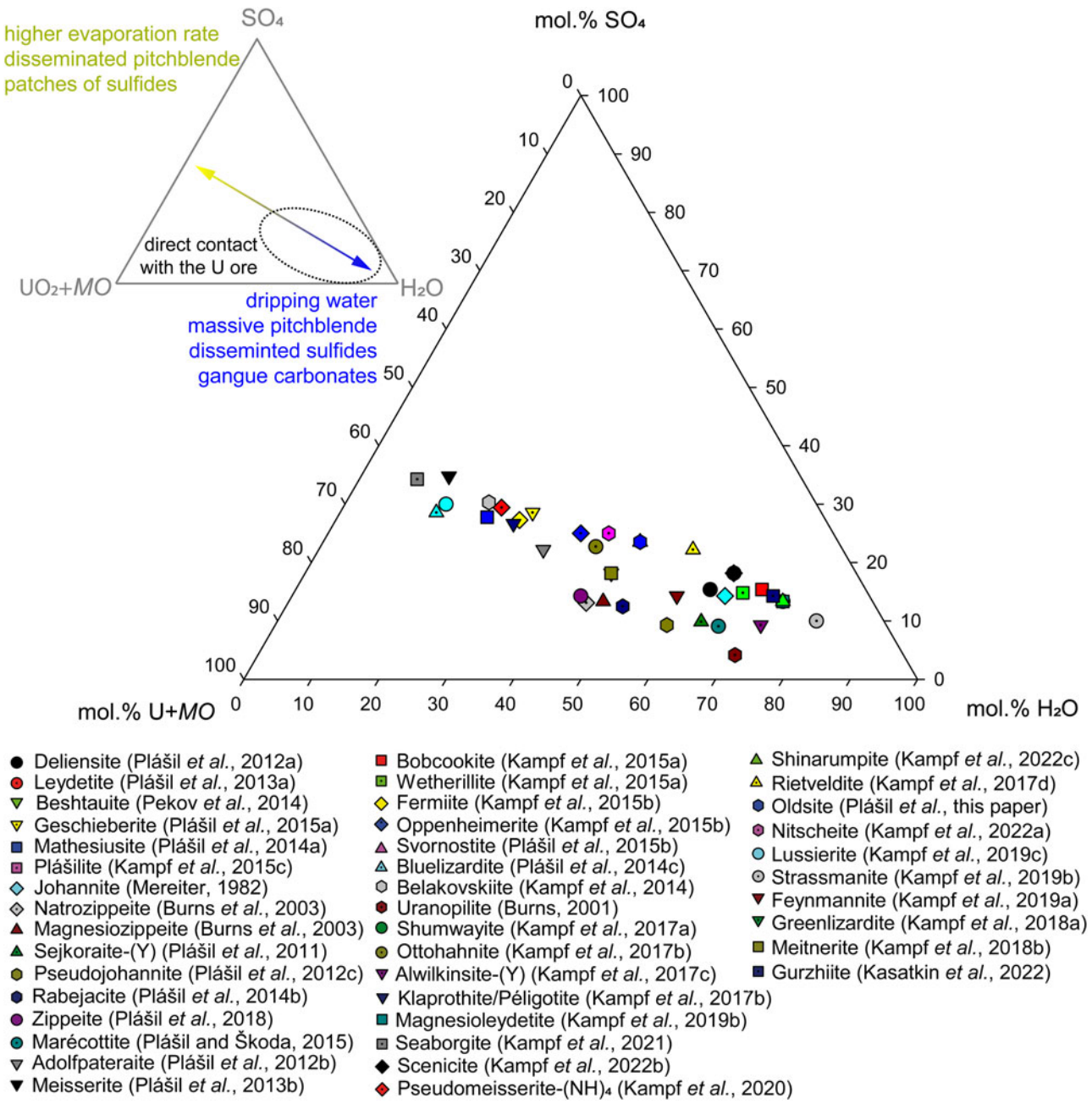

Fig. 5. Ternary diagram showing the composition of the 42 well-characterised uranyl sulfate minerals. References: Burns, 2001; Burns *et al*., 2003; Kampf *et al*., 2014, 2015a, 2015b, 2015c, 2017a, 2017b, 2017c, 2017d, 2018a, 2018b, 2019a, 2019b, 2019c, 2020, 2021, 2022a, 2022b, 2022c; Kasatkin *et al*., 2022, Mereiter, 1982; Pekov *et al*., 2014; Plášil *et al*., 2011, 2012a, 2012b, 2012c, 2013a, 2013b, 2014a, 2014c, 2015a, 2015b; Plášil and Škoda, 2015.

that uranyl sulfate minerals are relatively common in the post-mining assemblages of uranium mines, until recently, these assemblages had been largely overlooked and surprisingly, few natural uranyl sulfate phases were previously known and defined as valid mineral species. This situation began to change in 2012. Since then, many new uranyl sulfates have been discovered and described (Fig. 4).

Increases in the rate of new mineral descriptions are often attributed to technological advances (Barton, 2019). However, the last two decades have seen a significant jump forward in analytical techniques, especially related to X-ray and electron diffraction, enabling the analysis of much smaller crystals, measuring only a few tens of micrometres across or even smaller. This includes the more common use of electron diffraction tomography (or 3D electron diffraction) (Gemmi and Lanza, 2019; Gemmi *et al*., 2019). Indeed, these advances have contributed to the rapid increase in the number of well-characterised new uranyl sulfate minerals.

Perhaps of greater impact, however, has been the recognition that studies of low-temperature uranyl phases provide highly valuable insights into the transport of uranium in environmental systems. In the past, scientists investigating ore deposits tended to overlook or only superficially consider post-mining mineral assemblages, focusing on ore minerals and their formation

https://doi.org/10.1180/mgm.2022.106 Published online by Cambridge University Press

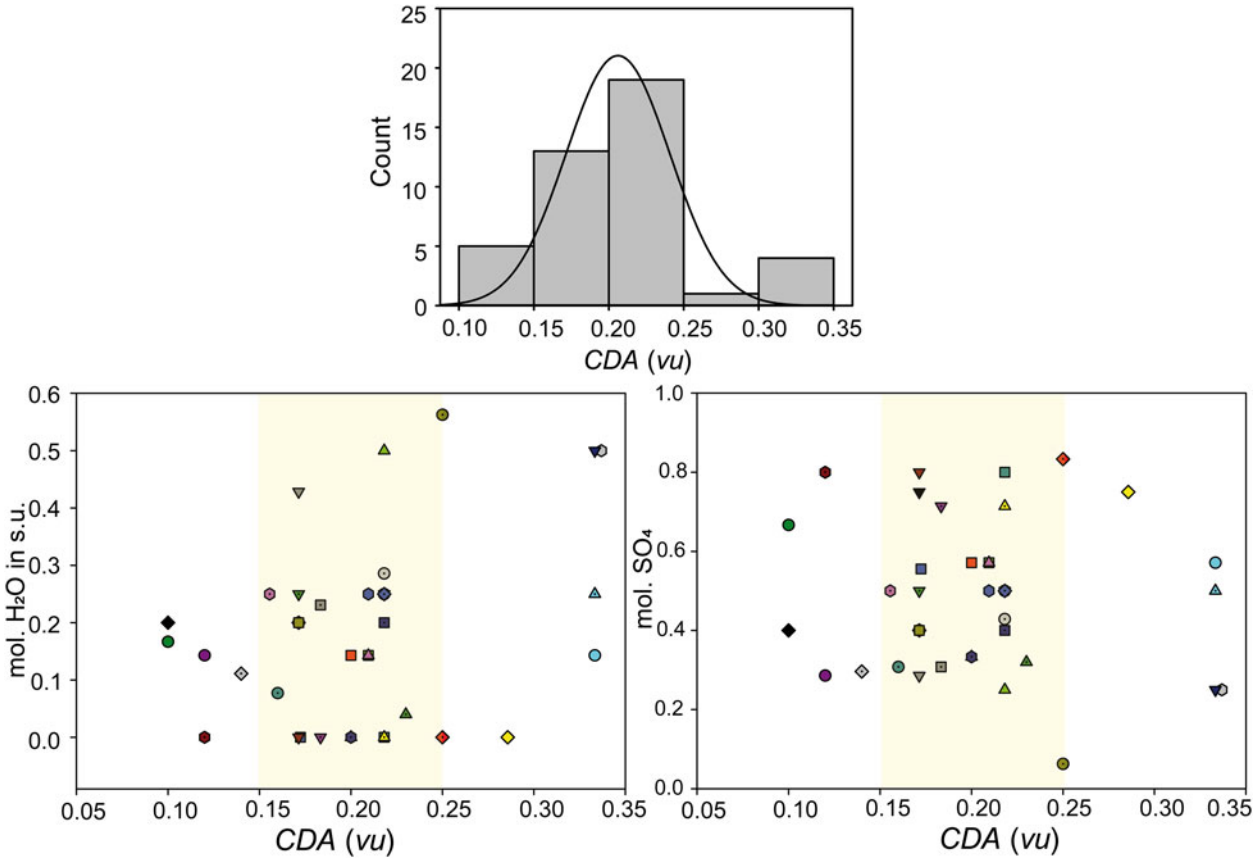

Fig. 6. The structural units of 42 well-characterised uranyl sulfate minerals characterised by the charge-deficiency per anion (*CDA*) value and its relationship with the molar proportion of the H_2O and SO_4 in the structural units (s.u.). The most frequent range of the *CDA* in uranyl sulfates (presented in the histogram above) is highlighted in both graphs (*CDA vs.* H_2O and *CDA vs.* SO_4) as yellow fields. See Fig. 5 for the key and reference list.

processes. For example, at Jáchymov (formerly known under the German name St. Joachimsthal) in the Czech part of Erzgebirge mountains, Schneeberg and Johanngeorgenstadt (in the German part of Erzgebirge), or Krunkelbach (Schwarzwald, Germany), studies generally focused on hydrothermal vein mineralisation. These localities (except for Krunkelbach) have been important to mineralogists since the start of mineralogy as a Science (see their original descriptions by the classical mineralogists Weissbach, Vogl, Schrauf and others in the 19th Century). The post-mining mineral associations at these deposits usually involve uranopilite, minerals of the zippeite group (undistinguishable at that time and considered as the single species zippeite) and schröckingerite. In the past, these minerals have often been referred to simply as 'uranium yellows or ochres'.

Unlike the occurrences noted above, sedimentary rocks play a prominent role in the U occurrences in the Lodève area, Hérault, Occitannie, France; nevertheless, the ore content (proportion of pitchblende *vs.* sulfidic ores), the gangue minerals and the properties of the surrounding rocks (notably, the buffering role of carbonates), as well as the climate (moderate, marine to continental), leads to the formation of similar mineral associations.

Since the description of meisserite (Plášil *et al.*, 2013b) from the Blue Lizard mine in Red Canyon of SE Utah (USA), the U deposits of the eastern Colorado Plateau region of the United States, also hosted by sedimentary rocks, have yielded an extensive suite of uranyl sulfates with unprecedented compositions and structural topologies. A ternary diagram (Fig. 5) displays the molar composition of 42 well-characterised uranyl sulfates, and Fig. 6 contains graphs of the charge deficiency-per-anion (*CDA*) with molar proportions of H_2O and SO_4 in structural units, both emphasising several important points that help elucidate the formation of uranyl sulfate minerals. The majority of the newly discovered uranyl sulfates from the Red Canyon area and other localities in Utah and Colorado, have medium to low H_2O content, high content of SO_4, and relatively low content of U, placing them in the central and the left portion of the ternary. For the solutions more concentrated in alkalis, and less so in U, a greater rate of evaporation (as documented by the field observations), leads to phases with high concentrations of Na and K (and other alkalis and alkaline earths) and lower H_2O content. The solutions from which these minerals crystallised can be viewed as micro-equivalents to those of Glauber Springs, the Western-Bohemian spa in Františkovy lázně city, known for Glauber's salt, $Na_2SO_4(H_2O)_{10}$. Referring back to Fig. 5, the mineral seaborgite, $LiNa_6K_2(UO_2)(SO_4)_5(SO_3OH)(H_2O)$ (Kampf *et al.*, 2021), can be regarded as kind of an end-member in so far as it has the lowest proportion of H_2O and a high content of alkaline cations (here also with Li), as well as a high proportion of SO_4. Interestingly, its *CDA* value of 0.18 valence units (vu), is not unusual among the uranyl sulfates (Fig. 6) when compared, e.g. to klaprothite, péligotite or meisserite. Their *CDA* values are very high (>0.30 vu) for uranyl oxysalts (e.g. Schindler and Hawthorne, 2008) and for oxysalts in general (Hawthorne and Schindler, 2008). This high value is related, to some extent, to the crystal-chemical stability of the structure within the chemical system

https://doi.org/10.1180/mgm.2022.106 Published online by Cambridge University Press

consisting of the components UO_7, SO_4, H_2O and Na. The most typical range in *CDA* for uranyl sulfates is 0.15 to 0.25 vu, reflecting again, to some extent, the pH range over which the structural units of these minerals are stable (see Hawthorne and Schindler, 2008 and references therein).

The minerals with high H_2O, high U (+ other cations) and lesser SO_4 contents dominate the lower right portion of the ternary (Fig. 5). Among these, it is uranopilite, $[(UO_2)_6(SO_4)O_2(OH)_6(H_2O)_6](H_2O)_8$ (Dauber, 1854; Vogl, 1856; Weisbach, 1882; Burns, 2001), which can be viewed as a transitional phase between pure uranyl-oxide hydroxy-hydrate minerals, such as schoepite, $[(UO_2)_4O(OH)_6](H_2O)_6$, and metal-cation-free uranyl sulfates, such as shumwayite, $[(UO_2)(SO_4)(H_2O)_2]_2{\cdot}H_2O$ (Kampf *et al.*, 2017b). Uranopilite is a typical alteration product of uraninite weathering in Jáchymov; uranopilite has been found growing directly on pitchblende lying in a small puddle at the foot-wall of the mining adit. Minerals such as straßmannite, gurzhiite, uranopilite, as well as johannite or deliensite, often occur in association with schröckingerite, $NaCa_3(UO_2)(CO_3)_3(SO_4)F{\cdot}10H_2O$ (Schrauf, 1873; Mereiter, 1986). This is another mineral that typically forms underground from water seepage on tunnel walls or associated with other uranyl carbonates (but also sulfates, such as zippeite-group minerals and uranopilite) at contact with mine waters and also in direct contact with the weathered surface of the pitchblende.

Acknowledgements. An anonymous referee, Associate Editor Mike Rumsey and Structure Editor Pete Leverett are highly thanked for their comments that helped improve the manuscript. A portion of this study was funded by the John Jago Trelawney Endowment to the Mineral Sciences Department of the Natural History Museum of Los Angeles County. This research was also financially supported by the Czech Science Foundation (project 20-11949S to JP).

Supplementary material. To view supplementary material for this article, please visit https://doi.org/10.1180/mgm.2022.106.

Competing interests. The authors declare none.

References

Bartlett J.R. and Cooney R.P. (1989) On the determination of uranium-oxygen bond lengths in dioxouranium(VI) compounds by Raman spectroscopy. *Journal of Molecular Structure*, **193**, 295–300.

Barton I.F. (2019) Trends in the discovery of new minerals over the last century. *American Mineralogist*, **104**, 641–651.

Brown I.D. (2002) *The Chemical Bond in Inorganic Chemistry. The Bond Valence Model*. Oxford University Press, Oxford, UK, 1–270 pp.

Brugger J., Meisser N. and Burns P.C. (2003) Contribution to the mineralogy of acid drainage of uranium minerals: marecottite and the zippeite-group. *American Mineralogist*, **88**, 676–685.

Burns P.C. (2001) A new uranyl sulfate chain in the structure of uranopilite. *The Canadian Mineralogist*, **39**, 1139–1146.

Burns P.C. (2005) U^{6+} minerals and inorganic compounds: insights into an expanded structural hierarchy of crystal structures. *The Canadian Mineralogist*, **43**, 1839–1894.

Burns P.C., Deely K.M. and Hayden L.A. (2003) The crystal chemistry of the zippeite group. *The Canadian Mineralogist*, **41**, 687–706.

Čejka J., Sejkora J., Mrázek Z., Urbanec Z. and Jarchovský T. (1996) Jáchymovite, $(UO_2)_8(SO_4)(OH)_{14}{\cdot}13H_2O$, A new uranyl mineral from Jáchymov, the Krušné Hory Mts., Czech Republic, and its comparison with uranopilite. *Neues Jahrbuch für Mineralogie-Abhandlungen*, **170**, 155–170.

Cordfunke E.H.P. (1972) The system uranyl sulphate-water—ii: Phase relationships and thermochemical properties of the phases in the system UO_3–SO_3–H_2O. *Journal of Inorganic and Nuclear Chemistry*, **34**, 1551–1561.

Dauber (1854) Untersuchungen an Mineralien der Sammlung des Hrn. Dr. Kranz in Bonn. *Annalen der Physik*, **92**, 237–251 [as Basisches Uransulphat].

Edwards K.J., Bond P.L., Druschel G.K., Mcguire M.M., Hamers R.J. and Banfield J.F. (2000) Geochemical and biological aspects of sulfide mineral dissolution: lessons from Iron Mountain, California. *Chemical Geology*, **169**, 383–397.

Evangelou V.P. and Zhang Y.L. (1995) A review - pyrite oxidation mechanisms and acid mine drainage prevention. *Critical Reviews in Environmental Science and Technology*, **25**, 141–199.

Gagné O.C. and Hawthorne F.C (2015) Comprehensive derivation of bond-valence parameters for ion pairs involving oxygen. *Acta Crystallographica*, **B71**, 562–578.

Gemmi M. and Lanza A.E. (2019) Electron diffraction techniques. *Acta Crystallographica*, **B75**, 495–504.

Gemmi M., Mugnaioli E., Gorelik T.E., Kolb U., Palatinus L., Boullay P., Hovmöller S. and Abrahams J.P. (2019) Electron diffraction: The nanocrystallography revolution. *ACS Central Science*, **5**, 1315–1329.

Gunter M.E., Bandli B.R., Bloss F.D., Evans S.H., Su S.C. and Weaver R. (2004) Results from a McCrone spindle stage short course, a new version of EXCALIBR, and how to build a spindle stage. *The Microscope*, **52**, 23–39.

Gurzhiy V.V. and Plášil J. (2019) Structural complexity of natural uranyl sulfates. *Acta Crystallographica*, **B75**, 39–48.

Hawthorne F.C. and Schindler M. (2008) Understanding the weakly bonded constituents in oxysalt minerals. *Zeitschrift für Kristallographie*, **223**, 41–68.

Kampf A.R., Plášil J. and Kasatkin A. (2014) Belakovskiite, $Na_7(UO_2)(SO_4)_4(SO_3OH)(H_2O)_3$, a new uranyl sulfate mineral from the Blue Lizard mine, San Juan County, Utah, USA. *Mineralogical Magazine*, **78**, 639–649.

Kampf A.R., Plášil J., Kasatkin A.V. and Marty J. (2015a) Bobcookite, $NaAl(UO_2)_2(SO_4)_4{\cdot}18H_2O$, and wetherillite, $Na_2Mg(UO_2)_2(SO_4)_4{\cdot}18H_2O$, two new uranyl sulfate minerals from the Blue Lizard mine, San Juan County, Utah, USA. *Mineralogical Magazine*, **79**, 695–714.

Kampf A.R., Plášil J., Kasatkin A.V., Marty J. and Čejka J. (2015b) Fermiite, $Na_4(UO_2)(SO_4)_3{\cdot}3H_2O$ and oppenheimerite, $Na_2(UO_2)(SO_4)_2{\cdot}3H_2O$, two new uranyl sulfate minerals from the Blue Lizard mine, San Juan County, Utah, USA. *Mineralogical Magazine*, **79**, 1123–1142.

Kampf A.R., Kasatkin A.V., Čejka J. and Marty J. (2015c) Plášilite, $Na(UO_2)(SO_4)(OH){\cdot}2H_2O$, a new uranyl sulfate mineral from the Blue Lizard mine, San Juan County, Utah, USA. *Journal of Geosciences*, **60**, 1–10.

Kampf A.R., Plášil J., Kasatkin A.V., Marty J. and Čejka J. (2017a) Klaprothite, péligotite and ottohahnite, three new sodium uranyl sulfate minerals with bidentate UO_7–SO_4 linkages from the Blue Lizard mine, San Juan County, Utah, USA. *Mineralogical Magazine*, **80**, 753–779.

Kampf A.R., Plášil J., Kasatkin A.V., Marty J., Čejka J. and Lapčák L. (2017b) Shumwayite, $[(UO_2)(SO_4)(H_2O)_2]_2{\cdot}H_2O$, a new uranyl sulfate mineral from Red Canyon, San Juan County, Utah, USA. *Mineralogical Magazine*, **81**, 273–285.

Kampf A.R., Plášil J., Čejka J., Marty J., Škoda R. and Lapčák L. (2017c) Alwilkinsite-(Y), a new rare-earth uranyl sulfate mineral from the Blue Lizard mine, San Juan County, Utah, USA. *Mineralogical Magazine*, **81**, 895–907.

Kampf A.R., Sejkora J., Witzke T., Plášil J., Čejka J., Nash B.P. and Marty J. (2017d) Rietveldite, $Fe(UO_2)(SO_4)_2(H_2O)_5$, a new uranyl sulfate mineral from Giveaway-Simplot mine (Utah, USA), Willi Agatz mine (Saxony, Germany) and Jáchymov (Czech Republic). *Journal of Geosciences*, **62**, 107–120.

Kampf A.R., Plášil J., Nash B.P. and Marty J. (2018a) Greenlizardite, $(NH_4)Na(UO_2)_2(SO_4)_2(OH)_2{\cdot}4H_2O$, a new mineral with phosphuranylite-type uranyl sulfate sheets from Red Canyon, San Juan County, Utah, USA. *Mineralogical Magazine*, **82**, 401–411.

Kampf A.R., Plášil J., Nash B.P. and Marty J. (2018b) Meitnerite, $(NH_4)(UO_2)(SO_4)(OH){\cdot}2H_2O$, a new uranyl-sulfate mineral with a sheet structure. *European Journal of Mineralogy*, **30**, 999–1006.

Kampf A.R., Olds T.A., Plášil J., Marty J. and Perry S.N. (2019a) Feynmanite, a new sodium–uranyl–sulfate mineral from Red Canyon, San Juan County, Utah, USA. *Mineralogical Magazine*, **83**, 153–160.

Kampf A.R., Plášil J., Kasatkin A.V., Nash B.P. and Marty J. (2019b) Magnesioleydetite and straßmannite, two new uranyl sulfate minerals with sheet structures from Red Canyon, Utah. *Mineralogical Magazine*, **83**, 349–360.

Kampf A.R., Olds T.A., Plášil J., Nash B.P. and Marty J. (2019c) Lussierite, a new sodium-uranyl-sulfate mineral with bidentate UO_7–SO_4 linkage from the Blue Lizard mine, San Juan County, Utah, USA. *Mineralogical Magazine*, **83**, 799–808.

Kampf A.R., Olds T.A., Plášil J., Nash B.P. and Marty J. (2020) Pseudomeisserite-(NH_4), a new mineral with a novel uranyl-sulfate linkage from the Blue Lizard mine, San Juan County, Utah, USA. *Mineralogical Magazine*, **84**, 435–443.

Kampf A.R., Olds T.A., Plášil J., Marty J., Perry S.N., Corcoran L. and Burns P.C. (2021) Seaborgite, $LiNa_6K_2(UO_2)(SO_4)_5(SO_3OH)(H_2O)$, the first uranyl mineral containing lithium. *American Mineralogist*, **106**, 105–111.

Kampf A.R., Olds T.A., Plášil J., Nash B.P. and Marty J. (2022a) Nitscheite, $(NH_4)_2[(UO_2)_2(SO_4)_3(H_2O)_2]\cdot 3H_2O$, a new mineral with an unusual uranyl-sulfate sheet. *American Mineralogist*, **107**, 1174–1180.

Kampf A.R., Plášil J., Olds T.A., Ma C. and Marty J. (2022b) Scenicite, a new uranyl-sulfate mineral from the White Canyon district, San Juan County, Utah, USA. *Mineralogical Magazine*, **86**, 743–748.

Kampf A., Plášil J., Olds T., M, C. and Marty J. (2022c) Shinarumpite, a new cobalt uranyl sulfate mineral from the Scenic mine, San Juan County, Utah, USA, structurally related to leydetite. *Mineralogical Magazine*, **87**, https://10.1180/mgm.2022.128

Kasatkin A.V., Plášil J., Chukanov N.V., Škoda R., Nestola F., Agakhanov A.A. and Belakovskiy D.I. (2022) Gurzhiite, $Al(UO_2)(SO_4)_2F\cdot 10H_2O$, a new uranyl sulfate mineral with chain structure from Bykogorskoe deposit, Northern Caucasus, Russia. *Mineralogical Magazine*, **86**, 412–421.

Krivovichev S.V. and Plášil J. (2013) Mineralogy and crystallography of uranium. Pp. 15–119 in: *Uranium, from Cradle to Grave* (P.C. Burns and G.E. Sigmon, editors). Mineralogical Association of Canada Short Course, 43. Mineralogical Association of Canada, Québec, Canada.

Leroy J.-M., Tudo J. and Tridot G. (1965) Sur les hydrates du sulfate d'uranyle. *Comptes Rendus Hebdomadaires des Séances de L'Académie Des Sciences*, **260**, 5802–5805.

Libowitzky E. (1999) Correlation of O–H stretching frequencies and O–H···O hydrogen bond lengths in minerals. *Monatshefte für Chemie*, **130**, 1047–1059.

Ling J., Sigmon G.E., Ward M., Roback N. and Burns P.C. (2010) Syntheses, structures, and IR spectroscopic characterization of new uranyl sulfate/selenate 1D-chain, 2D-sheet and 3D framework. *Zeitschrift für Kristallographie*, **225**, 230–239.

Mandarino J.A. (1976) The Gladstone-Dale relationship – Part 1: derivation of new constants. *The Canadian Mineralogist*, **14**, 498–502.

Mandarino J.A. (2007) The Gladstone–Dale compatibility of minerals and its use in selecting mineral species for further study. *The Canadian Mineralogist*, **45**, 1307–1324.

Mereiter K. (1982) Die Kristallstrukturs des Johannits, $Cu(UO_2)_2(OH)_2(SO_4)_2\cdot 8H_2O$. *Tschermaks Mineralogische und Petrographische Mitteilungen*, **30**, 47–57.

Mereiter K. (1986) Crystal structure and crystallographic properties of a schröckingerite from Joachimsthal. *Tschermaks Mineralogische und Petrographische Mitteilungen*, **35**, 1–18.

Pekov I.V., Krivovichev S.V., Yapaskurt V.O., Chukanov N.V. and Belakovskiy D.I. (2014) Beshtauite, $(NH_4)_2(UO_2)(SO_4)_2\cdot 2H_2O$, a new mineral from Mount Beshtau, Northern Caucasus, Russia. *American Mineralogist*, **99**, 1783–1787.

Petříček V., Dušek M. and Palatinus L. (2020) *Jana2020. The Crystallographic Computing System*. Institute of Physics, Prague, Czech Republic.

Plášil J. (2014) Oxidation-hydration weathering of uraninite: The current state-of-knowledge. *Journal of Geosciences*, **59**, 99–114.

Plášil J. and Škoda R. (2015) New crystal-chemical data for marécottite. *Mineralogical Magazine*, **79**, 649–660.

Plášil J., Dušek M., Novák M., Čejka J., Císařová I. and Škoda R. (2011) Sejkoraite-(Y), a new member of the zippeite group containing trivalent cations from Jáchymov (St. Joachimsthal), Czech Republic: description and crystal structure refinement. *American Mineralogist*, **96**, 983–991.

Plášil J., Hauser J., Petříček V., Meisser N., Mills S.J., Škoda R., Fejfarová K., Čejka J., Sejkora J., Hloušek J., Johannet J.-M., Machovič V. and Lapčák, L. (2012a) Crystal structure and formula revision of deliensite, Fe $[(UO_2)_2(SO_4)_2(OH)_2](H_2O)_7$. *Mineralogical Magazine*, **76**, 2837–2860.

Plášil J., Hloušek J., Veselovský F., Fejfarová K., Dušek M., Škoda R., Novák M., Čejka J., Sejkora J., Ondruš P. (2012b) Adolfpateraite, $K(UO_2)(SO_4)(OH)(H_2O)$, a new uranyl sulphate mineral from Jáchymov, Czech Republic. *American Mineralogist*, **97**, 447–454.

Plášil J., Fejfarová K., Wallwork K.S., Dušek M., Škoda R., Sejkora J., Čejka J., Veselovský F., Hloušek J., Meisser N. and Brugger J. (2012c) Crystal structure of pseudojohannite, with a revised formula, $Cu_3(OH)_2[(UO_2)_4O_4(SO_4)_2](H_2O)_{12}$. *American Mineralogist*, **97**, 1796–1803.

Plášil J., Kasatkin A.V., Škoda R., Novák M., Kallistová A., Dušek M., Skála R., Fejfarová K., Čejka J., Meisser N., Goethals H., Machovič V. and Lapčák L. (2013a) Leydetite, $Fe(UO_2)(SO_4)_2(H_2O)_{11}$, a new uranyl sulfate mineral from Mas d'Alary, Lodève, France. *Mineralogical Magazine*, **77**, 429–441.

Plášil J., Kampf A.R., Kasatkin A.V., Marty J., Škoda R., Silva S. and Čejka J. (2013b) Meisserite, $Na_5(UO_2)(SO_4)_3(SO_3OH)(H_2O)$, a new uranyl sulfate mineral from the Blue Lizard mine, San Juan County, Utah, USA. *Mineralogical Magazine*, **77**, 2975–2988.

Plášil J., Veselovský F., Škoda R., Novák M., Sejkora J., Čejka J., Škácha P. and Kasatkin A.V. (2014a) Mathesiusite, $K_5(UO_2)_4(SO_4)_4(VO_5)(H_2O)_4$, a new uranyl vanadate-sulfate from Jáchymov, Czech Republic. *American Mineralogist*, **99**, 625–632.

Plášil J., Dušek M., Čejka J. and Sejkora J. (2014b) The crystal structure of rabejacite, the Ca^{2+}-dominant member of the zippeite group. *Mineralogical Magazine*, **57**, 1249–1263.

Plášil J., Kampf A.R., Kasatkin A.V. and Marty J. (2014c) Bluelizardite, $Na_7(UO_2)(SO_4)_4Cl(H_2O)_2$, a new uranyl sulfate mineral from the Blue Lizard mine, San Juan County, Utah, USA. *Journal of Geosciences*, **59**, 145–158.

Plášil J., Hloušek J., Kasatkin A.V., Škoda R., Novák M. and Čejka J. (2015a) Geschieberite, $K_2(UO_2)(SO_4)_2(H_2O)_2$, a new uranyl sulfate mineral from Jáchymov. *Mineralogical Magazine*, **79**, 205–216.

Plášil J., Hloušek J., Kasatkin A.V., Novák M., Čejka J. and Lapčák L. (2015b) Svornostite, $K_2Mg[(UO_2)(SO_4)_2]_2\cdot 8H_2O$, a new uranyl sulfate mineral from Jáchymov, Czech Republic. *Journal of Geosciences*, **60**, 113–121.

Plášil J., Petříček V., Mills S.J., Favreau G. and Galea-Clolus V. (2018) Zippeite from Cap Garonne, France: an example of reticular twinning. *Zeitschrift für Kristallographie-Crystalline Materials*, **233**, 861–865.

Plášil J., Kampf A.R., Ma C. and Desor J. (2021) Oldsite, IMA 2021-075. CNMNC Newsletter 64. *Mineralogical Magazine*, **85**, https://doi.org/10.1180/mgm.2021.93

Schindler M. and Hawthorne F.C. (2008) The stereochemistry and chemical composition of interstitial complexes in uranyl-oxysalt minerals. *The Canadian Mineralogist*, **46**, 467–501.

Schindler M., Hawthorne F.C., Huminicki D.M.C., Haynes P., Grice J.D. and Evans H. (2003) Bobjonesite, V^{4+} O (SO_4) $(H_2O)_3$, a new mineral species from Temple Mountain, Emery County, Utah, U.S.A. *The Canadian Mineralogist*, **41**, 83–90.

Schrauf A (1873) Schröckingerit, ein neues Mineral von Joachimsthal. *Tschermaks Mineralogische und Petrographische Mitteilungen*, **1**, 137–138.

Sheldrick G.M. (2015) *SHELXT* – Integrated space-group and crystal-structure determination. *Acta Crystallographica*, **A71**, 3–8.

Škácha P., Plášil J. and Horák V. (2019) *Jáchymov – A Mineralogical Pearl of Krušné Hory Mts*. Academia, Praha, Czech Republic, 682 pp. [in Czech].

Tabachenko V.V., Serezhkin V.I., Serezhkina L.B. and Kovba L.M (1979) Crystal structure of manganese sulfatouranylate $MnUO_2(SO_4)_2(H_2O)_5$. *Koordinatsionnaya Khimiya*, **5**, 1563–1568.

Vogl J.F. (1856) *Gangverhältnisse und Mineralreichthum Joachimsthals*. J. W. Pöhlig Verlag, 200 s. Teplitz, Czech Republic [in German].

Weisbach A. (1882) Mineralogische Notizen II. 17. Uranocher. *Neues Jahrbuch für Mineralogie*, **2**, 258–259 [in German].

Zalkin A., Ruben H. and Templeton D.H. (1978) Structure of a new uranyl sulfate hydrate. α-$2UO_2SO_4\cdot 7H_2O$. *Inorganic Chemistry*, **17**, 3701–3702.